J. Electrochem. Sci. Eng. **15(4)** (2025) 2707; http://doi.org/10.5599/jese.2707

Open Access : : ISSN 1847-9286
www.jESE-online.org

Original scientific paper

Cathode intramolecular electron transfer of the Braga-Goodenough Li-S rechargeable battery

Masanori Sakai✉

Tenjinbayashicho 1225-144, Hitachiota-shi, Ibaraki 313-0049, Japan

Corresponding author: ✉ sakaimasanori144@gmail.com; *Tel: +81 807179 3084; Fax: +81 29473 1880*

Received: March 11, 2025; Accepted: May 20, 2025; Published: June 4, 2025

Abstract

Braga-Goodenough all-solid-state Li-S discharges beyond the theoretical capacity of the S_8 cathode and deposits Li during discharge, and the paradigm-shifting phenomena have been analysed by the previous mechanism. The mechanism has explained the phenomena coherently, except for an intrinsic question raised for the Li deposition step. This paper reviews and revises the previous mechanism and presents a new mechanism involving intramolecular tunnelling electron transfer within an adsorbate to clarify and resolve the issue. The formation of the adsorbate $S_8^-Li^+_{(sf)}(ad)$ (sf-surface states) is essential and characteristic, being the common step for both mechanisms. Since this adsorbate electron energy level is around the S_8^- or S_8 cathode potential range, the previous mechanism showed that electrons from the Li anode reduced $Li^+_{(sf)}(ad)$ in the $S_8^-Li^+_{(sf)}(ad)$ to deposit Li. However, this electron flow followed the established concept of battery discharge and raised the question of why the reduction path was not through S_8^-, but only through $Li^+_{(sf)}(ad)$ in the adsorbate. The present new mechanism answers this question through the tunnelling electron transfer from S_8^- to $Li^+_{(sf)}(ad)$ within the adsorbate, which is entirely congruent with the heterojunction physics analysis, and demonstrates a new overall reaction equation. Maximum Li deposition cycles and discharge capacity are also discussed.

Keywords

Li battery; lithium-sulphur; all-solid-state battery; reaction mechanism; Li deposition

List of symbols

Li-S	lithium-sulphur all-solid-state rechargeable battery
Na-Fc	sodium-ferrocene all-solid-state rechargeable battery
Li-MnO_2	lithium-manganese dioxide all-solid-state rechargeable battery
Li^+gl^-	Li-glass solid electrolyte of $Li_{2.99}Ba_{0.005}O_{1+x}Cl_{1-2x}$
Na^+gl^-	Na-glass solid electrolyte of $Na_{2.99}Ba_{0.005}O_{1+x}Cl_{1-2x}$
$Li^+_{(sf)}$	Li^+ in surface states of $Li_{2.99}Ba_{0.005}O_{1+x}Cl_{1-2x}$
$Na^+_{(sf)}$	Na^+ in surface states of $Na_{2.99}Ba_{0.005}O_{1+x}Cl_{1-2x}$
(sf)	surface states

$S_8^-Li^+_{(sf)}$ (ad)	adsorbed molecule between S_8^- and $Li^+_{(sf)}$
$Li^+_{(sf)}$ (ad)	$Li^+_{(sf)}$ in the adsorbate $S_8^-Li^+_{(sf)}$ (ad)
SOMO	single occupied molecular orbital
p, p-value	stoichiometric coefficient, number of $Li^+_{(sf)}$ available for adsorption, $p \geq 1$
E	electrochemical reaction
C	chemical reaction
C_E	intramolecular tunnelling electron transfer
$(ECC_E)n$	cathode reaction mechanism of Braga-Goodenough Li-S with C_E
n in $(ECC_E)n$	number of cycles of the (ECC_E) process and Li deposition, $p \geq n$
E[(ECC)c]n [7]	cathode reaction mechanism of Braga-Goodenough Li-S without C_E
n in E[(ECC)c]n [7]	number of cycles of the (ECC)c process and Li deposition, $p \geq n$
c in E[(ECC)c]n [7]	catalytic reaction steps
F	the Faraday constant
x_0	closest distance between $Li^+_{(sf)}$ and S_8^-
E_f	Fermi level
LUMO	lowest unoccupied molecular orbital
ϕ^G_{CNL}	generalized charge neutrality level
ϕ_{CNL}	charge neutrality level
$\|t_{VB\text{-}CB'}\|$	transfer energy between the valence band orbital of S_8^- and the conduction band orbital of $Li^+_{(sf)}$
$\|t_{VB'\text{-}CB}\|$	transfer energy between the valence band orbital of Li^+gl^- and the conduction band orbital of S_8^-
E_{CB}	energy level of the conduction band bottom for S_8^-
E_{VB}	energy level of the valence band top for S_8^-
E'_{CB}	energy level of the conduction band bottom for $Li^+_{(sf)}$ of Li^+gl^-
E'_{VB}	energy level of the valence band top for Li^+gl^-
E'_g	band gap, $E'_{CB} - E'_{VB}$, for Li^+gl^-
D_{VB}	density of states of the valence band for S_8^-
D_{CB}	density of states of the conduction band for S_8^-
D'_{VB}	density of states of the valence band for Li^+gl^-
D'_{CB}	density of states of the conduction band for $Li^+_{(sf)}$ of Li^+gl^-
Ψ	$(\|t_{VB\text{-}CB'}\|^2/\|t_{VB'\text{-}CB}\|^2)$ (D_{VB}/D_{CB})
S_{S8}/S_{Li+}	ratio of total surface area for $2x_0$ extended unit crystal lattice of S_8 to circle area in Li^+ radius
f_S	ratio of the area actually occupied by $Li^+_{(sf)}$ on the adsorption surface
f_P	1 - porosity of cathode active mass/100
M_{eff}	effective moles or effective molality of S_8
M_{mes}	measured moles or measured molality of S_8
λ	utilization coefficient, M_{eff}/M_{mes}
p_{max}	maximum number of $Li^+_{(sf)}$ adsorbable on S_8^-
Q	discharge capacity of Li-S cathode
Q_{max}	maximum discharge capacity of Li-S cathode
high-k	high relative permittivity

Introduction

The specific capacity 3860 mAh/g of Li is more than 10 times higher than that of the cathodes of lithium-ion batteries, and alkali metal rechargeable batteries are still expected to be the next-generation energy devices. In order to take advantage of the high specific capacity of alkali metals, it is essential to develop cathode active materials with high specific capacity. Sulphur, which has a specific capacity of 1670 mAh/g, more than six times that of lithium-ion cathodes, is one of the candidates for future cathode active materials [1].

In 2017, Braga *et al.* [2] presented Li-S, Na-Fc and Li-MnO_2 all-solid-state alkali metal rechargeable batteries, which exhibited distinctly divergent battery phenomena compared with conventional batteries. These batteries utilized glass solid electrolytes containing alkali metal ions ($Li_{0.99}Ba_{0.005}O_{1+X}Cl_{1-2X}$ or $Na_{0.99}Ba_{0.005}O_{1+X}Cl_{1-2X}$) developed by them [2]. These Braga-Goodenough batteries have two main features: firstly, alkali metals are deposited in the cathode active masses during discharge, and secondly, the discharge capacity of the battery greatly exceeds the theoretical capacity of the cathodes. Specifically for Li-S in the three batteries, Braga *et al.* provided the most detailed data [2]. In particular, the full discharge test data clearly demonstrated the above two features and indicated that the Li anode was the capacity-determining electrode [2]. These two features of the Braga-Goodenough batteries are far beyond the battery functionality expected from an extension of conventional Li-S development concepts.

Prior to the advent of the Braga-Goodenough batteries, no one could anticipate or understand a battery that could demonstrate a discharge capacity exceeding the theoretical capacity of either the cathode or the anode, or an alkali metal battery that could demonstrate its alkali metal deposition in the cathode active mass during discharge. It is imperative to acknowledge and reaffirm that the observed phenomena exhibited by the Braga-Goodenough batteries were such that their results could be difficult to accept based on the prevailing conventional understanding of battery phenomena at the time [3]. Therefore, these phenomena were all surprising to us and of such significance that they were considered paradigm shifts.

In order to comprehend the aforementioned two features, it was first necessary to elucidate the reaction mechanisms for the deposition of alkali metals in the cathode active masses. These reaction mechanisms also had to be able to explain the second characteristic, the fact that every battery capacity exceeded the theoretical capacity of the cathode. However, at the time of the advent of the Braga-Goodenough batteries, there was no reaction equation that could adequately describe the discharge phenomena of alkali metal deposition in the cathode active masses [3]. As a result, it was initially impossible to understand these battery phenomena in terms of reaction mechanisms [2-6].

One of the main reasons for the lack of understanding of the cathode reactions seems to be the lack of analysis from a cross-disciplinary perspective, such as chemistry, electrochemistry, solid-state physics and heterojunction physics, as described in the preceding papers [7,8]. Different fields of expertise generally have different perspectives of analysis. However, as the same battery reactions are observed, the results of the analyses of the reaction mechanisms examined from the perspective of the respective disciplines are considered to contain elements that complement each other. Therefore, it is considered that there are common elements that allow results on reaction mechanisms from the viewpoints of chemistry and electrochemistry to share rationality with results on reaction mechanisms from the viewpoints of solid-state physics and heterojunction physics.

The alkali metal deposition reaction is usually written as $Li^+ + e \rightarrow Li$, taking Li deposition as an example. However, it is clear that this reaction does not proceed in the cathode potential range [3]. For alkali metal deposition to occur as spontaneous reactions at the cathodes, *i.e.* the condition for $\Delta G < 0$ with regard to the Gibbs' free energy change, the electron energy levels of the surface states of the alkali metal ions of Li^+gl^- and Na^+gl^- in the cathode active materials must be lower than those of the alkali metal ions in the anode active materials. This means that the surface states of the alkali metal ions of the Li^+gl^- and Na^+gl^- in the cathode active materials and those of the alkali metal ions in the anode active materials are chemically different.

On the basis of the experimental results of Braga *et al.* [2], the electron energy levels of alkali metal ions in the Li^+gl^- and Na^+gl^- surface states in the cathode active materials are considered to be

lowered to the electron energy levels of S_8, Fc and MnO_2, the potential-determining cathode active materials. Therefore, the major difference between the active materials of the cathodes and those of the anodes is the presence of S_8, Fc and MnO_2 in the cathode active materials and the absence of these in the anode active materials. Thus, the alkali metal ions of the Li^+gl^- and Na^+gl^- surface states in the cathode active materials are considered to be in a state where molecular orbital contact is possible through solid/solid contact with S_8, Fc and MnO_2, and the adsorption by this molecular orbital contact is considered to lower the electron energy levels of the alkali metal ions to the electron energy levels of S_8, Fc and MnO_2.

The investigation of the mechanisms for these three types of batteries commenced with Li-S [7], followed by Na-Fc and Li-MnO_2 [8]. As described above, the key elementary reactions for the deposition of alkali metals in these reaction mechanisms were identified as adsorption processes [7,8]. These adsorption processes were classified as chemisorption involving orbital contact and orbital hybridisation between either $Li^+_{(sf)}$ or $Na^+_{(sf)}$ and each of the potential-determining cathode active materials of S_8, Fc or MnO_2. In the case of Li-S, the adsorption process did not occur directly with S_8 but the reaction between S_8^- and $Li^+_{(sf)}$ [7], where S_8^- is an intermediate radical formed by the one-electron reduction of S_8. The electron energy level of the adsorbate $S_8^-Li^+_{(sf)}$(ad) between S_8^- and $Li^+_{(sf)}$ is located in the S_8^- or S_8 cathode potential range, thereby resulting in a significant reduction in the electron energy level of $Li^+_{(sf)}$(ad) in the adsorbate $S_8^-Li^+_{(sf)}$(ad).

In the preceding paper [7], it was considered that this reduction in electron energy level could initiate an electron transfer from the Li anode to the adsorbate $S_8^-Li^+_{(sf)}$(ad) [7]. In order for Li to be deposited in the cathode active mass in this mechanism, it was necessary for the electrons from the anode to enter the $Li^+_{(sf)}$(ad) side of the adsorbate $S_8^-Li^+_{(sf)}$(ad) [7]. On the other hand, in the case of Na-Fc and Li-MnO_2, it was considered that the alkali metal deposition could be ascribed to the intramolecular tunnelling electron transfer reactions in the adsorbates between Fc and $Na^+_{(sf)}$ and MnO_2 and $Li^+_{(sf)}$ [8].

Heterojunction physics, ϕ^G_{CNL} played an essential role in the investigation of these reaction mechanisms [7,8] (see Appendix). ϕ^G_{CNL} provided essential criteria for investigating the charge neutrality level in heterojunctions and for determining the possibility and direction of electron transfer between the components of the adsorbed molecules [7,8].

In accordance with the reaction mechanisms for Li-S, Na-Fc and Li-MnO_2, the discharge capacity and the deposition cycles of alkali metals were investigated [7,8]. The discharge capacity of these three batteries was found to be proportional to the number of deposition cycles of each alkali metal [7,8], and the deposition cycles of each alkali metal were found to depend on the effective number of $Li^+_{(sf)}$ or $Na^+_{(sf)}$ that could be adsorbed by the cathode active material of each battery [7,8].

Although in the Braga-Goodenough batteries, only the Li-S experimentally exhibited a discharge capacity exceeding 10 times the theoretical capacity of the S_8 cathode in its full discharge test [2], according to the mechanisms for Li-S, Na-Fc and Li-MnO_2 [7,8], it was also indicated that for all three batteries, the discharge capacity of each battery could be able to exceed 10 times the theoretical capacity of each cathode active material [7,8]. These mechanisms allowed us to understand the experimental results shown by Braga *et al.* that these batteries continued to discharge beyond the theoretical capacities of the cathode active materials and deposited alkali metals in the cathode active masses during discharge [2,7,8].

In the preceding paper [7], the mechanism of Li-S was summarized by the shorthand formula E[(ECC)c]*n*, in which E denoted an electrochemical step, C denoted a chemical step, c indicated catalytic steps, and *n* denoted the process of (ECC)c repeated *n* times. The catalytic part of the

reaction (ECC)c cycles the deposition of Li. That is, *n* denotes the number of cycles of the Li deposition step (ECC)c.

Although this E[(ECC)c]*n* mechanism was able to coherently explain the Braga-Goodenough Li-S phenomena, there remained an essential question raised for the Li deposition step corresponding to the E step in the (ECC)c part, as was already commented on in the preceding paper [7]. This question was why the electrons from the Li anode selectively reduced only $Li^+_{(sf)}$(ad) and not S_8^- in the adsorbate $S_8^-Li^+_{(sf)}$(ad). This flow of electrons from the Li anode to the cathode during discharge followed the established concept of battery discharge, and in the preceding paper [7], the rationale for the selectivity of the reduction only $Li^+_{(sf)}$(ad) in the adsorbate could not be rationally explained. The explanation was limited to the fact that Li was deposited in the cathode active mass during discharge [7].

This paper presents a new $(ECC_E)n$ mechanism, where C_E stands for the intramolecular tunnelling electron transfer step, *n* denotes the Li deposition cycles by repeating the (ECC_E) process, and E and C have their usual significance shown above. This $(ECC_E)n$ mechanism provides a solution to the question through the C_E process corresponding to the Li deposition step of the electron transfer from S_8^- to $Li^+_{(sf)}$(ad) within the adsorbate $S_8^-Li^+_{(sf)}$(ad). The diagnostic criteria in terms of ϕ^G_{CNL} in relation to this $(ECC_E)n$ mechanism are entirely congruent with this intramolecular tunnelling electron transfer.

As a result of revising the elementary reaction of Li deposition in terms of this $(ECC_E)n$ mechanism, the overall reaction equation appears to be different from that derived from the previous E[(ECC)c]*n* mechanism demonstrated in the preceding paper [7]. With regard to the overall battery reaction equations, they are generally a fundamental requirement for determining the battery design conditions in practical batteries. It is therefore concluded that the discrepancy in the overall battery reaction equations derived from the battery mechanism analyses is considered the most fundamental and crucial issue. Consequently, this $(ECC_E)n$ mechanism is considered a lynchpin in the understanding of Braga-Goodenough Li-S.

The present paper expounds on this $(ECC_E)n$ mechanism, comparing the results derived from the E[(ECC)c]*n* mechanism obtained in the preceding paper [7] and also delving into the subjects of maximum Li deposition cycles and discharge capacity.

Experimental

Since all contents of this paper are related to the reviews and revisions of the preceding paper [7], all experimental results for Li-S are referred to the data and descriptions in Braga *et al*. [2], which are the same as in the preceding paper [7]. Regarding the electronic states in terms of band gap, critical radius and density of states for the S_8 and the intermediate radical S_8^-, the data from the preceding paper [7] are employed in this paper, which were obtained by quantum chemical calculations with Gaussian 09, Revision E.01, with the accuracy of APFD/6-311+G(2d,p) [7]. Since S_8^- is a radical species, its calculations are expressed as SOMO calculations.

Results and discussion

$(ECC_E)n$ model

Figure 1 shows the Braga-Goodenough Li-S battery diagram, which reflects a picture of Li deposition in the following mechanism $(ECC_E)n$. The cathode active mass consists of the active materials of S_8 powder and Li^+gl^- powder and the current collectors of carbon black powder and Cu. In this Braga-Goodenough Li-S, as described in this section, Li^+gl^- acts not only as the battery separator but also as the reaction active material of the cathode. At the interfaces between the potential-

determining material S_8 and the solid glass electrolyte powder Li^+gl^-, Li is deposited in the active mass during discharge [2]. Instead of the intermediate radical S_8^- in the previous mechanism [7], S_8 is covered with deposited Li under discharge conditions in Figure 1.

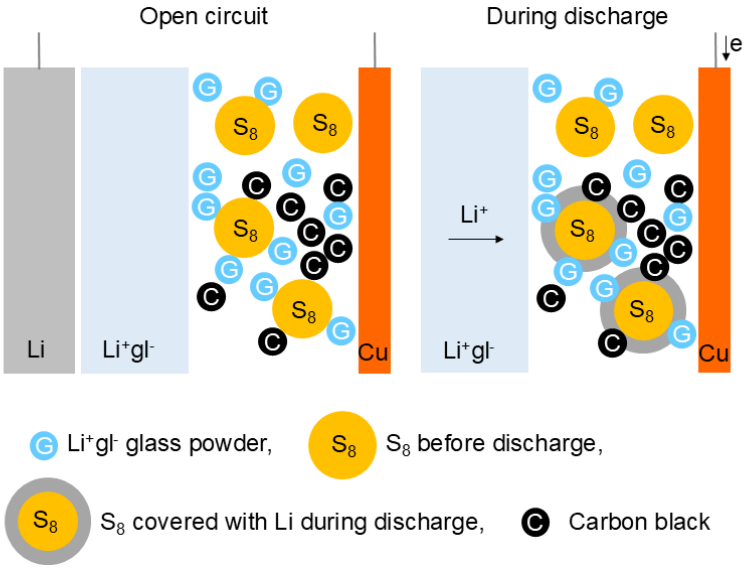

Figure 1. *Diagrams of the Braga-Goodenough Li-S cathode active mass under open circuit and discharge conditions reflecting the $(ECC_E)n$ mechanism. Instead of the intermediate radical S_8^- in the previous mechanism [7], S_8 is covered with deposited Li under discharge conditions*

Equations (1) to (9) are the elementary reactions of the Li-S cathode related to Li deposition during discharge. The first step, Equation (1), shows the one-electron electrochemical reduction of S_8, forming the intermediate S_8^-. The left side of Equation (1) shows that $pLi^+_{(sf)}$ for an S_8 will occupy the position where orbital contact and hybridisation are possible due to the solid-solid contact between S_8 and Li^+gl^-. In this paper, as was the case in the preceding paper on Na-Fc and Li-MnO_2 [8], the stoichiometric coefficient p, which is an integer and $p \geq 1$, is introduced. The p-value is defined as the number of initial states of $Li^+_{(sf)}$ that can be adsorbed on S_8^-. Equation (2) represents the equilibrium reaction, and the right side of the equation indicates that, among these $pLi^+_{(sf)}$, one $Li^+_{(sf)}$ with the highest probability of orbital contact and hybridisation at the interface with S_8^- forms the adsorbate molecule of $S_8^-Li^+_{(sf)}(ad)$.

$$E: \quad S_8\, pLi^+_{(sf)} + e \rightarrow S_8^-\, pLi^+_{(sf)} \qquad (1)$$

$$C: \quad S_8^-\, pLi^+_{(sf)} \leftrightarrow S_8^-\, Li^+_{(sf)}(ad)(p\text{-}1)Li^+_{(sf)} \qquad (2)$$

$$C_E: \quad S_8^-\, Li^+_{(sf)}(ad)(p\text{-}1)Li^+_{(sf)} \rightarrow S_8\, Li\, (p\text{-}1)Li^+_{(sf)} \qquad (3)$$

Equation (3) represents the intramolecular tunnelling electron transfer from S_8^- to $Li^+_{(sf)}(ad)$ in the adsorbate $S_8^-Li^+_{(sf)}(ad)(p\text{-}1)Li^+_{(sf)}$ resulting in the oxidation of S_8^- itself to S_8 and the reduction of $Li^+_{(sf)}(ad)$ to Li. This reaction step corresponds to the elementary reaction of Li deposition. Furthermore, S_8, which has been reduced to S_8^- in Equation (1), is regenerated in this intramolecular tunnelling electron transfer step, Equation (3). It can therefore be concluded that 1*F* (C) discharge per one mole of S_8 from Equations (1) through (3) results in the deposition of one mole of Li. The reactions described by Equations (1) to (3) correspond to the initial cycle of Li deposition.

The notations E, C and C_E correspond to the electrochemical, chemical and intramolecular tunnelling electron transfer reactions, respectively. The notation E of the electrochemical reaction here is defined as the electron transfer through current collectors from the Li anode. On the other hand, the C_E step corresponds to the electron transfer occurring directly within the adsorbate molecule in the form of tunnelling electron transfer between orbitals with the same electron energy

levels within the adsorbate. It is important to distinguish between these two steps, E and C_E. The adsorption process of Equation (2) and the intramolecular tunnelling electron transfer of Equation (3) are straightforwardly compatible with the ϕ^G_{CNL} analysis discussed in detail later in the next section.

The regenerated S_8 in the form of $S_8Li(p\text{-}1)Li^+_{(sf)}$ in Equation (3) re-initiates the subsequent discharge in the reaction schemes from Equations (4) to (6) as follows:

$$E: \quad S_8\ Li\ (p\text{-}1)Li^+_{(sf)} + e \rightarrow S_8^-\ Li\ (p\text{-}1)Li^+_{(sf)} \tag{4}$$

$$C: \quad S_8^-\ Li\ (p\text{-}1)Li^+_{(sf)} \leftrightarrow S_8^-\ [Li^+_{(sf)}(ad)]\ Li\ (p\text{-}2)Li^+_{(sf)} \tag{5}$$

$$C_E: \quad S_8^-\ [Li^+_{(sf)}(ad)]\ Li\ (p\text{-}2)Li^+_{(sf)} \rightarrow S_8\ 2Li\ (p\text{-}2)Li^+_{(sf)} \tag{6}$$

Equations (4), (5) and (6) correspond to the second cycle of Li deposition and are analogous to Equations (1), (2) and (3), respectively. The only difference is in the content of the notation; the *p*-value and the number of Li differ by one in each equation. The number of cycles of Li deposition and the number of moles of Li deposited correspond to the number of reductions of the *p*-value from its initial value *p*.

Since Equations (1) to (3) and Equations (4) to (6) correspond to the reaction pairs for the 1st and 2nd cycles of Li deposition, respectively, the discharge reaction proceeds by repeating these reaction pairs, decreasing the *p*-value by one and increasing the number of Li by one. When the number of cycles of these reaction pairs is *n*, then the *n*th Li deposition occurs in the *n*th cycle. Therefore, at the end of the *n*th cycle, the amount of discharge electricity and the number of moles of Li deposited are *nF* (C) and *n* moles, respectively, where *n* is an integer and $n \leq p$. As the first and the second reaction pairs correspond to Equations (1) to (3) and Equations (4) to (6), respectively, the following Equations (7) to (9) correspond to the reaction pair for the n^{th} cycle of Li deposition.

$$E: \quad S_8\ (n\text{-}1)Li\ (p\text{-}n\text{+}1)Li^+_{(sf)} + e \rightarrow S_8^-\ (n\text{-}1)Li\ (p\text{-}n\text{+}1)Li^+_{(sf)} \tag{7}$$

$$C: \quad S_8^-\ (n\text{-}1)Li\ (p\text{-}n\text{+}1)Li^+_{(sf)} \leftrightarrow S_8^-\ [Li^+_{(sf)}(ad)]\ (n\text{-}1)Li\ (p\text{-}n)Li^+_{(sf)} \tag{8}$$

$$C_E: \quad S_8^-\ [Li^+_{(sf)}(ad)]\ (n\text{-}1)Li\ (p\text{-}n)Li^+_{(sf)} \rightarrow S_8\ nLi\ (p\text{-}n)Li^+_{(sf)} \tag{9}$$

In this paper, on the basis of the above reaction equations, this reaction mechanism can be represented in terms of the shorthand formula $(ECC_E)n$.

By integrating the summation from Equations (1) to (9), the cathode overall reaction equation of Equation (10) for the *n*th Li deposition cycles in the cathode active mass can be obtained as follows:

$$S_8\ pLi^+_{(sf)} + ne \rightarrow S_8\ nLi\ (p\text{-}n)Li^+_{(sf)} \tag{10}$$

Figure 2 shows the schematic representation of the $(ECC_E)n$ mechanism. In Figure 2, for the reaction pairs described above, the reaction cycle is included up to $n = 2$, *i.e.* from Equations (1) to (6). For the number of Li deposition cycles, *i.e.* the intramolecular tunnelling electron transfer cycle, the number of cycles is included up to $n = 3$. In respect of the intramolecular tunnelling electron transfer, S_8^- is considered to play the essential role as an electron donor for $Li^+_{(sf)}(ad)$ and as a catalyst from the point of view of the reaction cycles of this $(ECC_E)n$ mechanism.

Figure 3 shows a schematic representation under $p = 10$ conditions, in which S_8^- contacts $Li^+_{(sf)}$, $Li^+_{(sf)}(ad)$ and the deposited Li under cycle 1 ($n = 1$) conditions in the left panel. The right panel of Figure 3 shows the diagram of the conditions following tunnelling electron transfer from S_8^- to $Li^+_{(sf)}(ad)$. As illustrated in Figure 3, the dimensions of S_8^-, S_8, $Li^+_{(sf)}$, $Li^+_{(sf)}(ad)$ and Li in each radius reflect those observed in practice, where the radii of $Li^+_{(sf)}$ and $Li^+_{(sf)}(ad)$ are represented by that of Li^+. Although the dimension of S_8^- is marginally larger than that of S_8, based on SOMO calculations [7], both sizes are represented as equivalent.

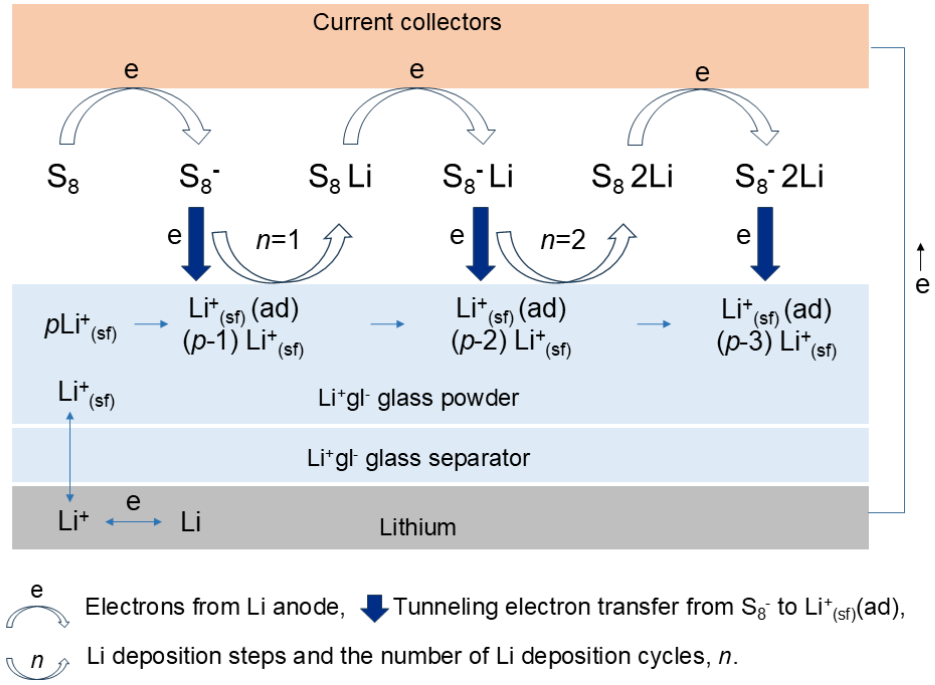

Figure 2. *Schematic representation of the Li deposition cycle in the (ECC$_E$)n mechanism for Braga-Goodenough Li-S. S_8 is first reduced to S_8^- by an electron from the Li anode, and one of the $Li^+_{(sf)}$ of the $pLi^+_{(sf)}$ adsorbs on this S_8^- radical. Once the adsorbate $S_8^-Li^+_{(sf)}$(ad) is formed, the intramolecular tunnelling electron transfer takes place, and S_8 is regenerated with Li deposition. These reactions are then repeated. Three filling arrows indicate the direction of the tunnelling electron transfer within the adsorbate $S_8^-Li^+_{(sf)}$(ad). The reaction cycle of the (ECC$_E$)n mechanism is included up to n = 2*

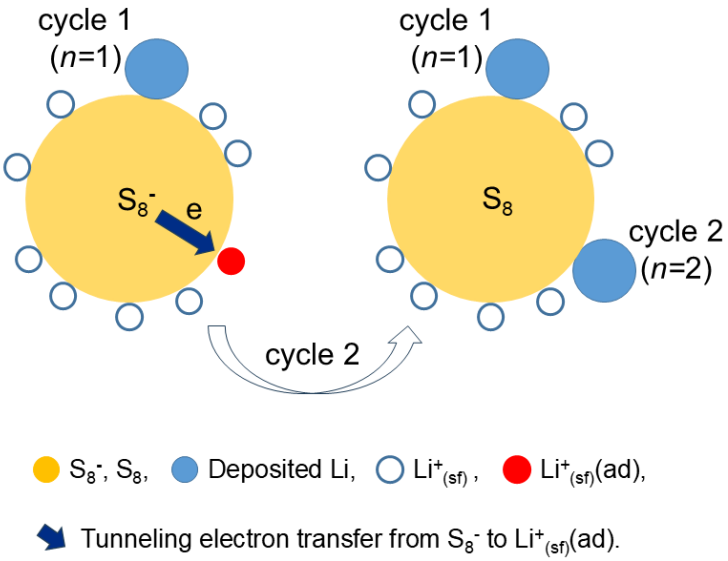

Figure 3. *Schematic representation of the intramolecular tunnelling electron transfer within $S_8^-Li^+_{(sf)}$(ad) including the sequence of the Li deposition cycle from n = 1 to n = 2 in the (ECC$_E$)n mechanism under p = 10 conditions. In the left panel, S_8^- functions to reduce $Li^+_{(sf)}$(ad) to Li, and in the right panel, S_8 is regenerated during the Li deposition cycle 2. As two cycles of Li deposition are already completed, the remaining p-value is (p-2) = 8. Under these conditions, this (ECC$_E$)n cycle is still capable of cycling further under these conditions, with an additional n = 8. The circle radii reflect those of 483 S_8^-, 59 $Li^+_{(sf)}$ and 152 Li in pm*

As demonstrated in Equation (10), when $p = 1$ ($p \geq 1$), the minimum conditions for the p-value yield the minimum Li deposition cycle $n = 1$. Hence, Equation (11) for the minimum Li deposition for the 1F (C) discharge is derived from Equation (10) by introducing $p = n = 1$.

$$S_8\ Li^+_{(sf)} + e \rightarrow S_8\ Li \qquad (11)$$

The maximum number of Li deposition cycles can be attained when $p = n$ ($p \geq n$) in Equation (10). Thus, Equation (12) is derived from Equation (10) by introducing $p = n$.

$$S_8\ pLi^+_{(sf)} + pe \rightarrow S_8\ pLi \quad (12)$$

For an ordinary Li-S, the cathode discharge capacity per one mole of S_8 is $2F$ (C) [7]. However, as demonstrated above in Equation (12), in the case of Braga-Goodenough Li-S, the discharge capacity of the cathode can reach up to pF (C) per one mole of S_8. As demonstrated above, the Li^+gl^- of the $Li^+_{(sf)}$ resource can be defined as the cathode active material of the Braga-Goodenough Li-S. The number of p-values is, therefore, like an indicator of the practical discharge capability of this battery. Determining the practical p-value is therefore one of the fundamental points in practical battery design when using this battery in practice. The following section describes the evaluation methodology and pragmatic evaluation of this p-value in practice.

With regard to the battery overall reaction involving the Li anode, these are explained below. The Li anode reactions paired with the cathode overall reaction in Equation (10) are Equations (13) and (14) as follows:

$$nLi \rightarrow nLi^+ + ne \quad (13)$$

$$nLi^+ \leftrightarrow nLi^+_{(sf)} \quad (14)$$

The Li anode overall reaction is then given by Equation (15) from the sum of Equations (13) and (14) as follows:

$$nLi \rightarrow nLi^+_{(sf)} + ne \quad (15)$$

Therefore, the overall reaction of Li-S is given by Equation (16) from the sum of Equations (10) and (15) as follows:

$$S_8\ pLi^+_{(sf)} + nLi \rightarrow S_8\ nLi\ (p\text{-}n)Li^+_{(sf)} + nLi^+_{(sf)} \quad (16)$$

In the case of $n = p$ under maximum discharge conditions for the cathode, Equation (16) is equal to Equation (17).

$$S_8\ pLi^+_{(sf)} + pLi \rightarrow S_8\ pLi + pLi^+_{(sf)} \quad (17)$$

Table 1 summarizes the cathode overall reactions of the two mechanisms, $(ECC_E)n$ and the previous E[(ECC)c]n [7], including the overall reactions for the Li anode and this battery. In the preceding paper [7], the adsorbate $S_8^-Li^+_{(sf)}$(ad), which appears in Equations [2], [5] and [8] of this paper, received electrons directly from the Li anode. This raised the aforementioned question of why the reduction path was not through S_8^-, but only through $Li^+_{(sf)}$(ad) in the adsorbate. This $(ECC_E)n$ mechanism provides a clear answer to the question through the intramolecular tunnelling electron transfer within the adsorbate $S_8^-Li^+_{(sf)}$(ad).

As shown in Table 1, these two mechanisms of this $(ECC_E)n$ and the previous E[(ECC)c]n exhibit divergent cathode and overall battery reaction equations. A difference in the overall reaction in the same battery leads to a different battery design in practical use. Therefore, this difference in overall reactions derived from their elementary reactions is of great importance and means an essential point in the research of reaction mechanisms.

Table 1. *Overall discharge reactions in each mechanism*

Mechanism	S_8 cathode	Li anode	Battery[a]
$(ECC_E)n$	$S_8\ pLi^+_{(sf)} + ne \rightarrow S_8\ nLi\ (p\text{-}n)Li^+_{(sf)}$	$nLi \rightarrow nLi^+_{(sf)} + ne$	$S_8\ pLi^+_{(sf)} + nLi \rightarrow S_8\ nLi\ (p\text{-}n)Li^+_{(sf)} + nLi^+_{(sf)}$
E[(ECC)c]n [7]	$S_8 + (n+1)Li^+_{(sf)} + (n+1)e \rightarrow S_8^-Li^+_{(sf)}$(ad) + nLi [7]	$(n+1)Li \rightarrow (n+1)Li^+_{(sf)} + (n+1)e$ [7]	$S_8 + Li \rightarrow S_8^-Li^+_{(sf)}$ [7]

[a]The overall discharge reaction is the sum of the overall discharge reactions of the S_8 cathode and the Li anode.

Table 2 summarizes the crucial reaction steps and thermodynamic factors of the two mechanisms in terms of Li deposition at the cathode, *i.e.* $\Delta G < 0$ and electron transfer. As shown in Table 2, the difference in electron transfer during Li deposition is the key point of distinction between the two mechanisms. In other words, in the previous E[(ECC)c]*n* mechanism, the conventional electron transfer during battery discharge, *i.e.* from the Li anode to the S_8 cathode, raises two possibilities in relation to the reduction of the adsorbate $S_8^-Li^+_{(sf)}$(ad). One is the reduction of $Li^+_{(sf)}$(ad), which can explain the Li deposition. The other is the reduction of S_8^-, which cannot explain the Li deposition and simply leads to the ordinary Li-S discharge reaction. These two possibilities raised in the previous mechanism are the essential point of the present paper. In the previous E[(ECC)c]*n* mechanism, it was not possible to choose the S_8^- reduction path because no Li deposition occurred along it. The present paper indicates that the lack of a rational explanation for this selection is ascribed to the original difference in the electron transfer mechanism for depositing Li. This present paper reveals that the intramolecular tunnelling electron transfer from S_8^- to $Li^+_{(sf)}$(ad) within the adsorbate $S_8^-Li^+_{(sf)}$(ad) is the step responsible for Li deposition during discharge.

Table 2. *Summary of the key points of the two mechanisms in relation to the cathode Li deposition*

Mechanism	Crucial reaction step for Li deposition	Thermodynamic rationale, $\Delta G < 0$ for Li deposition	Electron transfer for Li deposition
$(ECC_E)n$	Adsorbate formation of $S_8^-Li^+_{(sf)}$(ad)	Lower electron energy level of the adsorbate $S_8^-Li^+_{(sf)}$(ad) than the Li anode	Intramolecular tunnelling electron transfer[a]
E[(ECC)c]*n* [7]		Same as $(ECC_E)n$	Electron transfer *via* ordinary battery discharge[b]

[a]From S_8^- to $Li^+_{(sf)}$(ad) within the adsorbate $S_8^-Li^+_{(sf)}$(ad).
[b]From Li anode electrons to the adsorbate $S_8^-Li^+_{(sf)}$(ad) in the S_8 cathode.

The charging reactions of this $(ECC_E)n$ mechanism correspond to the reverse reactions of this mechanism. Under the conditions of a charge-discharge cycle, it is unlikely that the state of the distribution $Li^+_{(sf)}$ around S_8 after charging will be the same as before discharging [8]. It is natural to assume that the *p*-value, which appears as an initial value in Equation (1), may vary from cycle to cycle. From this point of view, it is considered that the self-charging phenomena described by Braga *et al.* [5,6,9] can be attributed to an increase of this *p*-value in Equation (1) from cycle to cycle as described in the preceding paper for Na-Fc and Li-MnO_2 [8].

Braga *et al.* described that the Braga-Goodenough Li-S was reversible, deposited Li in the cathode active mass and did not consume S_8 above the cell voltage of 2.34 V, as demonstrated by the 28-day full discharge capacity test [2]. Therefore, as long as their data is taken into account, this $(ECC_E)n$ mechanism is valid up to a cell voltage of 2.34 V, because at cell voltages below 2.34 V, Braga *et al*. described that S_8 started to be consumed [2]. From their experimental data [2], it can be seen that at a cell voltage of 2.34 V, the Li-S capacity exceeds eight times the theoretical S_8 capacity of the cathode. According to the results of this 28-day full discharge capacity test [2], the capacity-determining electrode was not the S_8 cathode but clearly the Li metal anode. This is also another unique feature of the Braga-Goodenough Li-S because in conventional alkali metal anode batteries, the capacity-determining electrodes are their cathodes.

It is thought that the relationship between the $(ECC_E)n$ mechanism and the Li-S cell voltage window during discharge depends on several factors, such as the preparation conditions of the cathode active mass, the practical charging and discharging rate, and so on. Therefore, this cell voltage of 2.34 V can be recognized as a kind of threshold to sustain the $(ECC_E)n$ mechanism.

According to this $(ECC_E)n$ mechanism, the discharge capacity will be nF (C) for n Li deposition cycles per S_8 within this $(ECC_E)n$ mechanism cell voltage window. Since an ordinary Li-S discharge capacity is $2F$ (C) per S_8, the total discharge capacity, including after the $(ECC_E)n$ mechanism is completed, will be $(n+2)F$ (C). Therefore, the ratio of the discharge capacity of the Braga-Goodenough Li-S to that of an ordinary Li-S is simply expressed by Equation (18) and Equation (19), without considering other factors such as the utilization coefficient, λ, of practical batteries, as follows:

$$100(n+2)/2 \quad (18)$$

$$100n/2 \quad (19)$$

Equations (18) and (19) correspond respectively to the full discharge test and the limited discharge test within the voltage range > 2.34 V, where the $(ECC_E)n$ mechanism takes place. These Equations (18) and (19) connote $\lambda = 1$ conditions and are basically identical to the findings from the E[(ECC)c]n mechanism in the preceding paper [7].

Until this Li-S cell voltage of 2.34 V of the discharge capacity test [2], the discharge amount of electricity of the battery already exceeds eight times the theoretical S_8 capacity [2]. In this case, within the $(ECC_E)n$ mechanism for Equation (19), the number of Li deposition cycles, n, is greater than 16. At the end of the full discharge test, the capacity was to exceed approximately 1100 % of the theoretical capacity of the S_8 cathode [2]. In this full discharge case, it is necessary from Equation (18) that the number of Li deposition cycles, n, is greater than 20. The practical significance of these Li deposition cycle values will be discussed in detail in the discharge capacity section.

For a good understanding of this $(ECC_E)n$ mechanism, it is essential to understand the adsorption processes of Equations (2), (5) and (8) and the intramolecular tunnelling electron transfer of Equations (3), (6) and (9). Adsorption processes involving orbital contacts between molecules are known to have a significant effect on their electron energy levels [10-13], and tunnelling electron transfer has been recognised as the basis of electron transfer reactions [14-16]. In the case of this $(ECC_E)n$ mechanism, the intramolecular tunnelling electron transfer, the C_E step, is thought to be the direct and elastic types of tunnelling electron transfer in the following [14-16].

Figure 4 shows that the electron energy levels of $Li^+_{(sf)}$ vary significantly with the distance from S_8^-. Regarding the electron energy levels of adsorbed particles, *i.e.* $Li^+_{(sf)}$ here, they are generally not the same as those of isolated particles [10-13]. The position of $pLi^+_{(sf)}$ in Equation (1) should be in the x_0 region in Figure 4, and this x_0 is considered to be around a 200 pm (0.2 nm) level, as described in the preceding paper for Na-Fc and Li-MnO_2 [8]. This 200 pm is based on the inner Helmholtz layer of the electric double layer structure, where the so-called specific adsorption and an inner-sphere electrode reaction take place [17]. This x_0 value is thus one of the key points in determining the maximum number of Li deposition cycles and the maximum discharge capacity of the Li-S cathode, as described in other sections.

Around this 200 pm, as shown in Figure 4, the electron energy levels between S_8^- and $Li^+_{(sf)}$ are considered to partially overlap, and tunnelling electron transfer of direct and elastic types occurs between the orbitals of S_8^- and $Li^+_{(sf)}$(ad) within the adsorbate $S_8^-Li^+_{(sf)}$(ad) [14-16]. Around 200 pm regions, the probability of electron transfer through an energy barrier is strongly dominated by the tunnelling effect [14-16]. On the other hand, taking into account the Boltzmann function, the probability of electron transfer through the energy barrier under these conditions can be recognised as zero [14-16].

S_8^- is the intermediate radical between the two consecutive one-electron reductions of S_8 to S_8^{2-}, the so-called EE mechanism [7]. In an EE mechanism, an intermediate radical has two levels in the frontier orbitals; one is occupied by electrons and the other is unoccupied [7,18,19]. In Figure 4, these

two levels of S_8^- are shown in two Gaussians of the probability distribution of density of states, and the Gaussian of the higher energy level corresponds to the orbital occupied by electrons. This is characteristic of an EE mechanism because the relationship between the energy levels of these two Gaussians is reversed compared with the ordinary redox couples, and the tunnelling of electrons from S_8^- to $Li^+_{(sf)}$(ad) is thought to be basically based on this orbital of the higher energy level Gaussian in Figure 4. The numbers on the y-axis were those estimated by taking into account the open circuit voltage and the measured potential of each anode and cathode of the Li-S [2]. Strictly speaking, the flat line of the Fermi level, E_f, from the current collectors to the adsorbate $S_8^-Li^+_{(sf)}$(ad) shown in Figure 4 may not seem realistic under battery discharge conditions. However, the expression in terms of flat E_f is useful to simplify the understanding of the overlap of the electron energy levels of the current collectors, S_8^- and $S_8^-Li^+_{(sf)}$(ad), to understand this $(ECC_E)n$ mechanism. In Figure 4, the shaded area shows the overlap of the electron energy distributions below E_f.

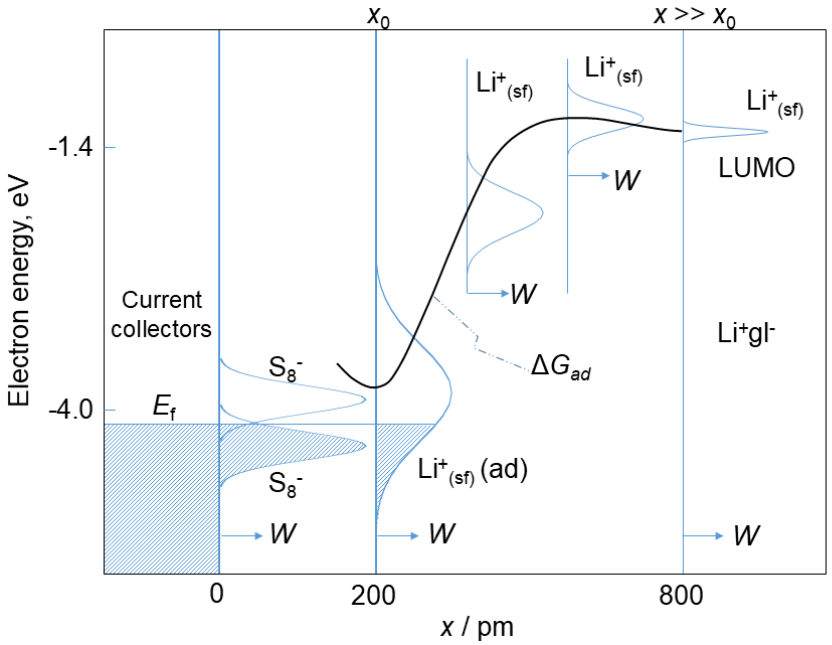

Figure 4. *Variation of electron energy levels of $Li^+_{(sf)}$ at various distances from S_8^-. As $Li^+_{(sf)}$ approaches S_8^-, the electron energy levels of $Li^+_{(sf)}$ approach S_8^- and spread out due to its interaction with S_8^-, having the widest probability density at x_0. ΔG_{ad}: adsorption energy curve of $Li^+_{(sf)}$ approaching S_8^-, W: probability density of electron energy states, x: distance to $Li^+_{(sf)}$, x_0: distance to adsorbed $Li^+_{(sf)}$ (ad). $Li^+_{(sf)}$ forms the adsorption bond with S_8^-, which significantly lowers the electron energy level of the adsorbed $Li^+_{(sf)}$. The electron energy level of $Li^+_{(sf)}$ decreases from the LUMO level of $Li^+_{(sf)}$ to the electron energy level range of S_8^- as $Li^+_{(sf)}$ approaches S_8^-, while its level width gradually widens [10,13]. The electron energy level width reaches its maximum at a distance of x_0 from S_8^- where orbital contact and hybridisation is possible with high probability [13]. At the same time, the adsorption energy curve, ΔG_{ad}, becomes the most stable energy state at x_0 [10,13]*

As described in detail in the next section, this $(ECC_E)n$ mechanism is straightforwardly compatible with the analysis of heterojunction physics ϕ^G_{CNL} and answers the question raised in the previous E[(ECC)c]*n* mechanism [7].

$(ECC_E)n$ mechanism from the perspective of ϕ^G_{CNL}

In this section, the $(ECC_E)n$ mechanism is analysed in terms of ϕ^G_{CNL}. As explained in the Appendix, the terminology of ϕ^G_{CNL} has been used in the field of semiconductor heterojunction physics and integrated circuit technology [20-24]. In the field of battery science, ϕ^G_{CNL} seems to be the first to be applied to the research mechanisms of these Braga-Goodenough batteries [7,8]. As will be shown in this section, ϕ^G_{CNL} basically demonstrates the charge neutrality level at a solid/solid contact

interface, which corresponds to a balanced electron energy level at the interface when two solid phases are in contact and is related to the Fermi levels on either side. Of particular interest are the evaluation capabilities of ϕ^{G}_{CNL} for solid/solid heterojunction interface properties in terms of charge transfer and orbital hybridisation [20-24].

With regard to the heterojunction interface between S_8^- and $Li^+_{(sf)}$, ϕ^{G}_{CNL} provides the two possibilities in terms of electron transfer and orbital hybridisation [20-24]. Figure 5 shows the two possibilities of electron transfer and orbital hybridisation in the theory of ϕ^{G}_{CNL} between S_8^- and Li^+gl^-. One is from the valence band of S_8^- to the $Li^+_{(sf)}$ conduction band of Li^+gl^-, and the other is from the O^{2-} and Cl^- valence bands of Li^+gl^- to the conduction band of S_8^-. In the first case, from the valence band of S_8^- to the $Li^+_{(sf)}$ conduction band, this is in direct agreement with the $(ECC_E)n$ mechanism and the experimental fact of Braga *et al*. [2] that Li is deposited in the cathode active mass during the discharge. Therefore, from the point of view of ϕ^{G}_{CNL}, the intramolecular tunnelling electron transfer within the adsorbate $S_8^-Li^+_{(sf)}$(ad) in the $(ECC_E)n$ mechanism is from the valence band of S_8^- to the conduction band of $Li^+_{(sf)}$(ad), as demonstrated by the bold line in Figure 5. With respect to the bands of Li^+gl^-, the conduction bands contain the frontier orbitals of Li^+ cations, and the valence bands comprise the frontier orbitals of O^{2-} and Cl^- in the glass electrolytes [25].

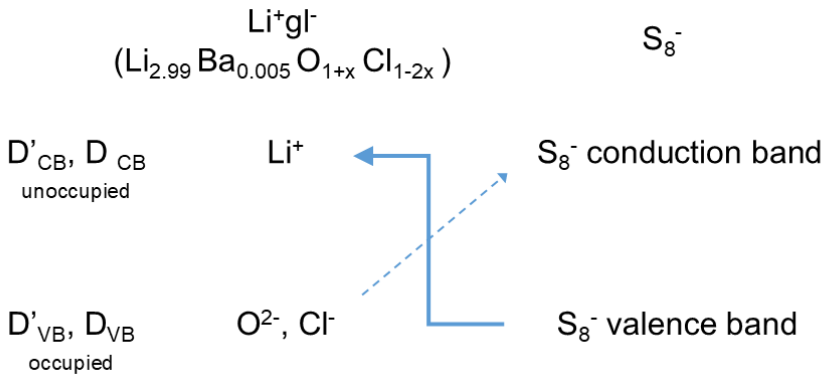

Figure 5. *Two possibilities of electron transfer and orbital hybridisation in the theory of ϕ^{G}_{CNL} between S_8^- and Li^+gl^-. The inset arrows indicate the direction of the possible electron transfer at their interfaces. D'_{CB} and D'_{VB} correspond respectively to the density of states of the conduction and valence bands of Li^+gl^-, and D_{CB} and D_{VB} correspond to the density of states of the conduction and valence bands of S_8^-. One is from the valence band of S_8^- to the $Li^+_{(sf)}$ conduction band of Li^+gl^-, and the other is from the O^{2-} and Cl^- valence bands of Li^+gl^- to the conduction band of S_8^-. The first case is consistent with the Li deposition of the experimental data of Braga et al. [2] and the $(ECC_E)n$ mechanism*

In the preceding paper [7], the focus of the deliberations on ϕ^{G}_{CNL} the charge neutral level and electron transfer in the heterojunction between S_8^- and $Li^+_{(sf)}$ was directed towards the formation of a dipole which induced a bias in the distribution of electrons within the adsorbed molecule from S_8^- to the $Li^+_{(sf)}$ side. However, the previous study did not encompass the mechanism of electron transfer within the adsorbate $S_8^-Li^+_{(sf)}$(ad) [7]. As shown here, the intramolecular tunnelling electron transfer from the valence band of S_8^- to the conduction band of $Li^+_{(sf)}$(ad) within the adsorbate $S_8^-Li^+_{(sf)}$(ad) is fully compatible with the theorem of heterojunction physics ϕ^{G}_{CNL} and this $(ECC_E)n$ mechanism. Therefore, the question raised in the E[(ECC)c]*n* mechanism obtained in the preceding paper [7] can be answered by this $(ECC_E)n$ mechanism.

Since the band gap of S_8^- is 0.64 eV based on SOMO calculations [7], as a usual level, S_8^- is considered to be a good electron conductor like carbon current collectors. Although in the preceding paper [7], S_8^- was treated as a metal-like material with a metal band structure, in this paper, S_8^- is

treated strictly as a semiconductor. Since Li^+gl^- is a typical insulator with high E'_g [2], the application of ϕ^G_{CNL} corresponds to the case of semiconductor-insulator interfaces. In this case, ϕ^G_{CNL} is given by Equation (20) as follows [8,20-24]:

$$\phi^G_{CNL} = E'_{VB} + E'_g|t_{VB'\text{-}CB}|^2 D_{CB}D'_{VB}/(|t_{VB'\text{-}CB}|^2 D_{CB}D'_{VB} + |t_{VB\text{-}CB'}|^2 D_{VB}D'_{CB}) \quad (20)$$

where E'_{VB}, E'_g, D'_{VB} and D'_{CB} are the level of the valence band top, the band gap, the valence band density of states and the conduction band density of states of Li^+gl^-, respectively; D_{VB} and D_{CB} are the valence band density of states and the conduction band density of states of S_8^-, respectively; $|t_{VB'\text{-}CB}|$ is the transfer energy between valence band orbitals of Li^+gl^- and conduction band orbitals of S_8^-; $|t_{VB\text{-}CB'}|$ is the transfer energy between valence band orbitals of S_8^- and conduction band orbitals of Li^+gl^-. The terms of $|t_{VB'\text{-}CB}|^2 D_{CB}D'_{VB}$ and $|t_{VB\text{-}CB'}|^2 D_{VB}D'_{CB}$ correspond to the effective bonding strengths at the heterojunction interface [24]. Although Li^+gl^- are amorphous structures, their band structures are expressed in terms of ordinary terminology because there is no obstacle in ϕ^G_{CNL} analyses of these reaction mechanisms [7,8,26].

The theory ϕ^G_{CNL} is built on an orbital hybridisation between the unoccupied and occupied states of two materials at an interface [20-24]. In this theory, as shown in Figure 5, the charge transfer between S_8^- and Li^+gl^- is realised by orbital hybridisation between their unoccupied and occupied states. The electron transfer is confined to just interfaces between S_8^- and Li^+gl^-.

Equation (20) can be obtained by solving $\Delta\rho = 0$ of Equation (21) with the unknown parameter E_f, which was derived by applying the second-order perturbation theory of quantum mechanics [22,27]. $\Delta\rho$ denotes the transfer charge from S_8^- to the insulator and is proportional to the right-hand side of the equation. At $\Delta\rho = 0$ in Equation (21), the E_f corresponds to the Fermi level and the charge neutrality level for S_8^- after contacting $Li^+_{(sf)}$ and is identical to ϕ^G_{CNL} of Equation (20).

$$\Delta\rho \propto D_{VB}D'_{CB}|t_{VB\text{-}CB'}|^2/(E'_{CB} - E_f) - D_{CB}D'_{VB}|t_{VB'\text{-}CB}|^2/(E_f - E'_{VB}) \quad (21)$$

where E'_{CB} corresponds to the conduction band bottom for $Li^+_{(sf)}$ of Li^+gl^- in this study.

Assuming $D_{VB} = D_{CB}$ and $|t_{VB\text{-}CB'}|^2 = |t_{VB'\text{-}CB}|^2$ in Equation (20), ϕ^G_{CNL} is consistent with the conventional charge neutrality level, ϕ_{CNL}, expressed in Equation (22) [28], and this ϕ_{CNL} is unable to demonstrate the effects of orbital hybridisation, adsorption, or electron transfer between S_8^- and $Li^+_{(sf)}$ [20-24].

$$\phi_{CNL} = E'_{VB} + E'_g D'_{VB}/(D'_{VB} + D'_{CB}) \quad (22)$$

In order to evaluate those effects, the magnitude of the second term on the right-hand side of Equation (20) is compared with Equation (22) to evaluate the difference in electron energy levels at heterojunction interfaces with and without orbital hybridisation.

In this study, let Equation (20), which is ϕ^G_{CNL}, be transformed into Equation (23) as follows [8]:

$$\phi^G_{CNL} = E'_{VB} + E'_g D'_{VB}/(D'_{VB} + \Psi D'_{CB}) \quad (23)$$

where $\Psi = (|t_{VB\text{-}CB'}|^2/|t_{VB'\text{-}CB}|^2)(D_{VB}/D_{CB})$. In comparing Equation (23) and Equation (22), $\phi^G_{CNL} < \phi_{CNL}$ corresponds to $\Psi > 1$, and $\phi^G_{CNL} > \phi_{CNL}$ corresponds to $\Psi < 1$. Therefore, the size relationship between ϕ_{CNL} and ϕ^G_{CNL} can be determined using Ψ. Therefore, depending on whether Ψ is greater than or less than 1, the difference in electron energy levels at heterojunction interfaces with and without orbital hybridisation and electron transfer can be evaluated.

First, $|t_{VB\text{-}CB'}|^2/|t_{VB'\text{-}CB}|^2$ in Ψ is examined. From Figure 5 and the experimental result of the Li deposition [2], the electron transfer based on ϕ^G_{CNL} is from the valence band of S_8^- to the conduction band of $Li^+_{(sf)}$(ad). Therefore, orbital hybridisation is strong between these bands, so that $|t_{VB\text{-}CB'}|^2 \gg |t_{VB'\text{-}CB}|^2$, *i.e.* $|t_{VB\text{-}CB'}|^2/|t_{VB'\text{-}CB}|^2 \gg 1$. With regard to the (D_{VB}/D_{CB}) of S_8^-, D_{VB} and D_{CB} in Ψ are considered almost equivalent on the basis of SOMO calculations. Considering these values of $|t_{VB\text{-}CB'}|^2/|t_{VB'\text{-}CB}|^2 \gg 1$ and $(D_{VB}/D_{CB}) = 1$, it can be concluded that Ψ is greater than one, $\Psi > 1$.

Therefore, it can be concluded that $\phi^{G}_{CNL} < \phi_{CNL}$, which is equivalent to the result previously obtained in the preceding paper [7].

Therefore, the electron energy level at the heterojunction interface with orbital hybridisation and electron transfer is obviously lower than without them. It is therefore considered that this finding indicates that when S_8^- and $Li^+_{(sf)}$ are in contact in the cathode active mass during discharge, the formation of adsorbed molecule $S_8^-Li^+_{(sf)}$(ad) and the associated intramolecular tunnelling electron transfer due to orbital hybridisation indicates more thermodynamically stable than when no orbital hybridisation and no electron transfer occurs.

In this paper, S_8^- is treated directly as a semiconductor; nevertheless, the result of the ϕ^{G}_{CNL} analysis remains consistent with that obtained in the preceding paper [7]. As shown in Figure 5, this $(ECC_E)n$ mechanism with the intramolecular tunnelling electron transfer from S_8^- to $Li^+_{(sf)}$(ad) within the adsorbate $S_8^-Li^+_{(sf)}$(ad) directly reflects the result of this ϕ^{G}_{CNL} analysis. Therefore, this $(ECC_E)n$ mechanism is entirely congruent with the ϕ^{G}_{CNL} analysis in terms of both the adsorbate formation and electron transfer processes. It is considered that if this result of the ϕ^{G}_{CNL} analysis had been directly reflected in the previous mechanism [7], the aforementioned question would not have arisen.

In the previous E[(ECC)c]*n* mechanism [7], the formation of the adsorbate $S_8^-Li^+_{(sf)}$(ad) is also compatible with the result of the ϕ^{G}_{CNL} analysis. However, the electron transfer reaction to deposit Li in the previous E[(ECC)c]*n* mechanism [7] is incompatible with the result of the ϕ^{G}_{CNL} analysis, which was based on the fixed idea of the electron flow path from the Li anode to the cathode. Since the electron energy level of the adsorbate $S_8^-Li^+_{(sf)}$(ad) is around that of the S_8^- or S_8 cathode potential range, therefore the idea of this electron flow itself is rational. However, as mentioned in the preceding paper [7], this electron flow of the E[(ECC)c]*n* mechanism could not rationally explain the reduction limited only to $Li^+_{(sf)}$(ad) in the adsorbate $S_8^-Li^+_{(sf)}$(ad). In other words, the E[(ECC)c]*n* mechanism could not explain why S_8^- in the $S_8^-Li^+_{(sf)}$(ad) could escape its reduction by the Li anode.

Maximum Li deposition cycle

On the basis of the $(ECC_E)n$ mechanism, the discharge capacity of the S_8 cathode is determined by the Li deposition cycles. In the case of Li deposition cycle $n = p$, as shown in Equation (12), the discharge capacity of the cathode reaches its maximum value. Therefore, the practical discharge capacity can be assessed by the effective number of the *p*-value under practical battery conditions. However, this p-value assessment is subject to a number of uncertainties; in fact, it depends on various factors of the actual battery cathode active mass itself. Therefore, the estimation of the Li-S discharge capacity for the cathode is evaluated taking into account several parameters that simulate practical active mass conditions.

In order to estimate a maximum number of Li deposition cycles, *n*, which in this paper is $n = p$, the critical radius of S_8^- in the preceding paper [7], was used to determine the effective number of $Li^+_{(sf)}$ for adsorption. The critical radius of S_8^- was calculated based on SOMO calculations, and the effective number of $Li^+_{(sf)}$ that could come into contact with the surface of the S_8^- sphere was calculated by considering the Li^+ ion radius and pragmatic preparation conditions of the cathode active mass [7].

In this paper, this *p*-value is evaluated using the unit crystal lattice size of S_8, which follows the same methodology as for Na-Fc and Li-MnO_2 in the preceding paper [8]. Although S_8 becomes S_8^- in its coordinates by one-electron reduction, the size of S_8^- shows a marginal increase in dimensions relative to S_8. In this paper, both sizes of S_8 and S_8^- are referred to as equivalent to each other. The proximity distance of $Li^+_{(sf)}$, which can be in orbital contact and orbital hybridisation with S_8^-, is set

to 200 pm. The number of $Li^+_{(sf)}$ available for adsorption onto S_8^- in the cathode active mass is the *p*-value itself, appearing in the $(ECC_E)n$ mechanism. As discussed in the previous section, the closest distance of $Li^+_{(sf)}$ to S_8^- is considered to be *ca.* 200 pm. It is therefore necessary to examine the *p*-value at this x_0 position in Figure 4. In this section, the *p*-value is to be evaluated by the following steps 1-4 as follows:

1. From the size of the unit crystal lattice of S_8, consider a new size lattice with axes that are extended by 200 pm each to the left, right, top and bottom of each axis of the unit crystal lattice for a total of 400 pm larger for each axis.
2. Find the total surface area of the new lattice size. Find the ratio of this total surface area to the area of the circle of radius *r* of $Li^+_{(sf)}$, expressed as (S_{S8}/S_{Li+}) for this (total surface area)/πr^2.
3. Introduce a factor f_S for the surface or volume factor, which is the fraction of the total surface of this large new lattice that is occupied by $Li^+_{(sf)}$, since the surface of the new lattice of S_8^- will be in common contact with the solid glass electrolyte as well as with the carbon current collector.
4. Introduce a factor f_P for the porosity of the cathode active mass, where f_P = [1- (porosity, % of cathode active mass) / 100].

From 1-4 above, in this paper, the maximum *p*-value, p_{max}, is obtained from the following Equation (24).

$$p_{max} = f_S f_P (S_{S8}/S_{Li+})/8 \quad (24)$$

The crystal structure of α-sulphur S_8 is of the orthorhombic type, and its lattice contains 16 of S_8 [29]. In Equation (24), therefore, $(S_{S8}/S_{Li+})/8$ means that half of the S_8 contained in the lattice is to be used for the adsorption, since the S_8 involved deep in the lattice cannot contact $Li^+_{(sf)}$. Therefore, this number of 8 cannot be considered as a fixed value and can be variable. In Equation (24), both f_S and f_P can also be variables.

Figure 6 shows an image of the ab plane projection of the S_8 orthorhombic crystal unit lattice with $Li^+_{(sf)}$ and deposited Li. The axes of the S_8 orthorhombic crystal unit lattice are a = 1046, b = 1287, c = 2449 pm [29], and the axis angles are $\alpha = \gamma = \beta = 90°$. In Figure 6, $Li^+_{(sf)}$ and Li total 33. Thus, in this case, the *p*-value in Equation (1) is at most 33. Two of these are shown depositing as Li on discharge. The first cycle of Li deposition corresponds to *n* = 1, and the second cycle corresponds to *n* = 2. In Figure 6, since 31 $Li^+_{(sf)}$ remains, when all of these are discharged, the number of cycles of Li deposition reaches a maximum at 33.

On the basis of step 2 above, (S_{S8}/S_{Li+}) is calculated directly as [2×(1446×1687)+2×(1446×2849)+ +2×(1687×2849)]/$59^2\pi$ = 2078. The radius of $Li^+_{(sf)}$ is replaced with 59 pm of Li^+. Radius data on Li^+ can be referred to elsewhere. In this paper, the values of f_S and f_P in Equation (24) are set to 1/3 and 0.5, respectively, as was previously employed in the preceding paper [7], and these values are considered pragmatic. Therefore, the p_{max} in Equation (24) is (1/3)×0.5×2078/8 = 43. Thus, the maximum number of Li deposition cycles under the above conditions in the $(ECC_E)n$ mechanism is expected to be $n = p_{max}$ = 43 as the utilization coefficient λ of $\lambda = 1$.

In the preceding paper [7], the maximum number of Li deposition cycles was 44. Despite the divergent evaluation methods in this section and the preceding paper [7], the maximum number of Li deposition cycles is considered equivalent. As described in the $(ECC_E)n$ mechanism section, this p_{max} is the key parameter to estimate the practical capability of the discharge capacity, taking into account practical values from $\lambda < 1$.

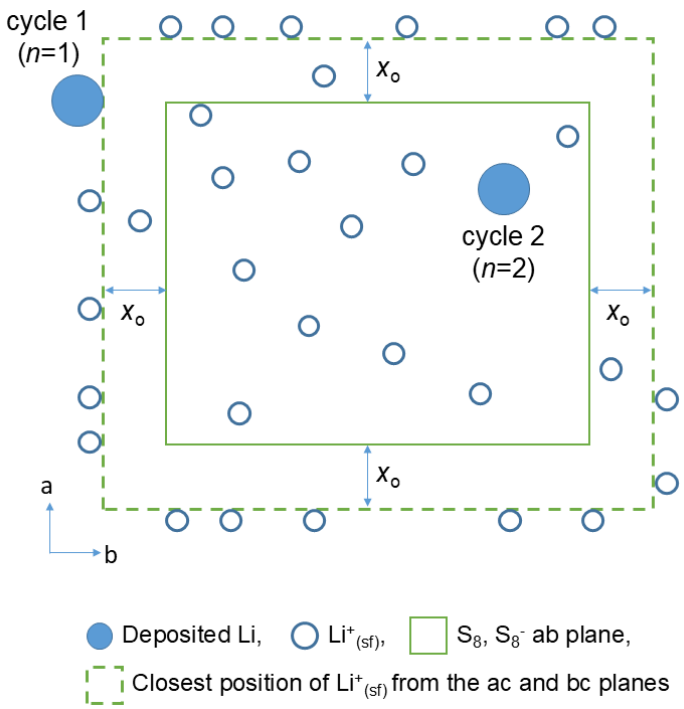

Figure 6. *An image of the ab plane projection of the S_8 orthorhombic crystal unit lattice with $Li^+_{(sf)}$ and deposited Li. Circles and filled circles correspond to adsorbable $Li^+_{(sf)}$ and deposited Li, respectively. Two filled circles correspond to Li deposition cycles 1 (n = 1) and 2 (n = 2). The circle radii reflect those of 152 Li and 59 Li^+ in comparison with the S_8 unit lattice axes of 1046 a and 1286 b in pm. x_0 is 200 pm, which is the closest distance of $Li^+_{(sf)}$ to the unit lattice. The dashed line corresponds to the solid line extended 200 pm to the left and right of the b axis and 200 pm above and below the a axis. $Li^+_{(sf)}$ and Li tangent to the dashed line are on the ac and bc planes. Other $Li^+_{(sf)}$ and Li are projected on the anterior ab plane without the posterior ab plane*

Table 3 summarizes the key points discussed in this section for each mechanism. Although λ was not directly employed in the previous E[(ECC)c]*n* mechanism [7], the evaluation of the maximum number of Li deposition cycles, *n*, essentially connotes $\lambda = 1$ conditions. Therefore, λ appears as $\lambda = 1$ for the E[(ECC)c]*n* mechanism in Table 3.

Table 3*. Maximum number of Li deposition cycles, n, and their evaluation methods with their parameters for each mechanism*

Mechanism	Maximum number of Li deposition cycles, *n*	Basic concept for each evaluation method of *n*	Parameters for each evaluation method of *n*	Parameter values
$(ECC_E)n$	43	Number of $Li^+_{(sf)}$ contacts on the surface of the S_8 unit lattice with 400 pm extended in each axis	S_{S8}/S_{Li}^+, f_S, f_p, λ and the number, *N*, of S_8 contactable with $Li^+_{(sf)}$ per S_8 unit lattice	$S_{S8}/S_{Li}^+ = 2078$ $f_S = 1/3$ $f_p = 0.5$ $\lambda = 1$ $1/N = 1/8$
E[(ECC)c]*n* [7]	44	Number of $Li^+_{(sf)}$ contacts on the surface of the sphere with critical radius S_8^-	S_{S8}^-/S_{Li}^+ corresponding to S_{S8}/S_{Li}^+ for $(ECC_E)n$, f_S, f_p and λ	$S_{S8}^-/S_{Li}^+ = 266$ $f_S = 1/3$ $f_p = 0.5$ $\lambda = 1$

Discharge capacity

The discharge capacity can be expressed simply using Equation (25) as follows:

$$Q = \lambda M_{mes} pF \text{ (C, C/kg)} \quad (25)$$

where λ is the utilization coefficient $\lambda = M_{eff}/M_{mes}$; M_{eff} is the effective molality (mol/kg) of S_8 or the effective number of moles of S_8, and M_{mes} is the measured moles or measured molality of S_8 at the stage of preparation of the cathode active mass. The discharge capacity Q reaches its maximum value of Q_{max} at $p = p_{max}$ in Equation (25). In practical batteries, $0 < \lambda < 1$, which mathematically implies the limits of $\lambda = 0$ and 1 [8]. Although the Li deposition cycles of $n = 16$ and $n = 20$ are demonstrated in the $(ECC_E)n$ mechanism section in relation to the discharge test data of Braga *et al*., these n values are essentially only verified under the conditions specified for the limit of $\lambda = 1$. Therefore, the practical Li deposition cycles in their discharge test [2] are larger than $n = 16$ and $n = 20$ because $\lambda < 1$. In the following, the p-value and λ are analysed using the experimental Li-S discharge data from Braga *et al*. [2].

Here the λp value in Equation(25) can be determined experimentally because the Li-S discharge test of Braga *et al*. was performed with the M_{mes} = 1.99 mg of S_8 at 47 wt% in the cathode active mass [2]. The theoretical capacity of the 1.99 mg = 7.77 μ mol of S_8 is 1.50 C or 0.416 mAh. Therefore, the capacity of the 8 times 7.77 μ mol of S_8 is 12.0 C or 3.33 mAh. Hence, λp = 16.0 is obtained from Equation (25), taking into account Q = 12.0 C, M_{mes} = 7.77 μ mol and F = 96500 (C/mol).

In consideration of the finding that λp = 16.0, in the case of p_{max} = 43 shown above, λ becomes 0.37. Therefore, taking these conditions into account, λ and p-values are considered to be constrained to the ranges of values $0.37 \le \lambda < 1$ and $16 < p \le 43$ under their Li-S discharge test conditions [2]. Since λp = 16.0, assuming λ has plausible values of 0.5 and 0.7, the p-values are 32 and 23, respectively.

As is well known, λ is one of the most important battery design parameters in practical batteries and depends on various factors of the active mass preparation conditions, *e.g.* its porosity, particle sizes of active materials of S_8 and Li^+gl^-, mesh number of carbon powder, wt % of each component, active mass layer thickness, *etc*. In addition, λ is also contingent upon a number of factors inherent in the configuration of the battery, including a low or high rate of use of discharge or charge.

For this $(ECC_E)n$ mechanism to proceed, the orbitals of $Li^+_{(sf)}$ of Li^+gl^- must maintain contact with those of S_8 and S_8^-. Practical particles of S_8 prepared in the cathode active mass are present as clusters of the S_8 unit lattice, which means that S_8 contained inside the clusters cannot participate in contacting the orbitals of $Li^+_{(sf)}$ of Li^+gl^- powder in the cathode active mass. This influence, like the size effect on λ, has already appeared in p_{max} in Equation (24). That is, in Equation (24), half the number of S_8 contained in the S_8 unit crystal lattice is only taken into account for contact with $Li^+_{(sf)}$.

These cathode reaction mechanisms of the Braga-Goodenough batteries are divergent from those of ordinary batteries. Therefore, in the preceding paper, for Na-Fc and Li-MnO_2 [8], λ has been analysed in principle, reflecting these mechanisms with the modelling of overlapping patterns and shapes of the clusters of the unit lattices for Fc and MnO_2. On the basis of these analyses, λ was considered to have its upper levels in the order of 0.7 to 0.8.

When this Li-S reaches the battery preparation conditions for λ = 0.7 and p-value = 43 of p_{max}, λp_{max} becomes 30.1, which is 1.88 times λp of 16 obtained experimentally above. Therefore, in this case of λp_{max} = 30.1, the maximum discharge capacity of Q_{max} = 22.6 C in Equation (25) is expected to be 1.88 times the Q = 12.0 C corresponding to the above experimental λp = 16. However, under λp = 16 discharge conditions, the Li anode was already 90.1 % discharged and the capacity-determining electrode of the Li-S [2]. Therefore, in order to achieve the above maximum discharge corresponding to λp_{max} = 30.1, the Li anode must have sufficient capacity to provide the value of the λp_{max}. This battery design condition, where the Li anode capacity balance is greater than the capacity of its cathode, is absolutely peculiar compared to conventional alkali metal anode batteries.

Consequently, although the maximum discharge capacity of the cathode is limited by p_{max} = 43 with a specific λ, in the case of λ = 0.7, Q_{max} = 22.6 C for λp_{max} = 30.1 can be realistic when Braga *et al.* used the much higher capacity Li anode than their Li-S in the discharge test [2].

In the preceding Li-S paper [7], λ was not taken into account. Although λ was not employed in the E[(ECC)c]*n* mechanism [7], not only the maximum number of Li deposition cycles but also the discharge capacity essentially connoted λ = 1 conditions. Therefore, a direct comparison of the mechanisms of this paper $(ECC_E)n$ and the preceding paper E[(ECC)c]*n* [7] cannot be made with regard to the discharge capacity of the cathode using λ.

Table 4 summarizes the key points discussed above for each mechanism. Although λ was not directly employed in the E[(ECC)c]*n* mechanism [7], the evaluations of not only the maximum number of Li deposition cycles in the preceding section, but also the discharge capacity, essentially connote λ = 1 conditions. Therefore, λ appears as λ = 1 for the E[(ECC)c]*n* mechanism in Table 4.

***Table 4**. Discharge capacity Q in each mechanism*

Mechanism	Q	Q_{max}	Q_{max} at λ = 0.7	λ
$(ECC_E)n$	$12\lambda p/16$[a] (C)	$12\lambda p_{max}/16$[a] (C) with p_{max}=43	12×0.7×43/16=22.6 (C)	Variable
E[(ECC)c]*n* [7]	Not generally applicable			Constant, 1

[a]As shown in the $(ECC_E)n$ mechanism section, the discharge capacity in the cell voltage range > 2.34 V is experimentally more than 8 times the theoretical S_8 capacity [2]. As shown in the discharge capacity section, the experimentally determined λp = 16.0 corresponds to 12 C of 8 times the theoretical S_8 capacity.

Conclusions

This paper has reviewed and revised the cathode reaction mechanism of the Braga-Goodenough Li-S, which deposited Li in the cathode active mass and exhibited a discharge capacity exceeding the theoretical capacity of the S_8 cathode during discharge, and presents a revised new $(ECC_E)n$ mechanism. This $(ECC_E)n$ repeats the Li deposition in the C_E step of the intramolecular tunnelling electron transfer corresponding to the number of Li deposition cycles, *n*. In the previous E[(ECC)c]*n* mechanism, an intrinsic question arose in the Li deposition step and was left unanswered. This revised $(ECC_E)n$ mechanism has answered the question why electrons from the Li anode did not choose the reduction path of S_8^-, but only $Li^+_{(sf)}$(ad) in the adsorbate $S_8^-Li^+_{(sf)}$(ad), taking into account of the intramolecular tunnelling electron transfer.

The two mechanisms were basically identical up to the formation step of the adsorbate $S_8^-Li^+_{(sf)}$(ad). From a heterojunction physics point of view, the result of the ϕ^G_{CNL} analysis was consistent with this adsorbate formation in both mechanisms. After this adsorbate formation, each mechanism was separated into two different types of Li deposition steps. In this $(ECC_E)n$ mechanism, the intramolecular tunnelling electron transfer from S_8^- to $Li^+_{(sf)}$(ad) to deposit Li occurs within the adsorbate $S_8^-Li^+_{(sf)}$(ad). This mechanism was also directly compatible with the diagnostic criteria of the ϕ^G_{CNL} analysis. Consequently, this $(ECC_E)n$ mechanism is entirely congruent with the ϕ^G_{CNL} analysis in terms of the adsorbate formation and electron transfer processes.

In the previous E[(ECC)c]*n* mechanism, it was assumed that the $Li^+_{(sf)}$(ad) in the adsorbate $S_8^-Li^+_{(sf)}$(ad) was directly reduced to Li by the Li anode, because the electron energy level of the $Li^+_{(sf)}$(ad) of the adsorbate $S_8^-Li^+_{(sf)}$(ad) was around that of the S_8^- or S_8 cathode potential range. This electron flow path is identical to that of a conventional battery discharge. However, this selection, which followed this fixed concept, was incompatible with the ϕ^G_{CNL} analysis and therefore left the above question unresolved.

This $(ECC_E)n$ mechanism demonstrates a different overall Li-S reaction equation from that derived from the previous E[(ECC)c]*n* mechanism. This fact is of great importance not only from a reaction mechanism point of view, but also from a practical battery design point of view, as the overall reaction equation of a battery is one of the most important essential parameters for battery design.

In this $(ECC_E)n$ mechanism, a maximum number of cycles, *n*, of Li deposition corresponds to the maximum discharge capacity and has been expressed in terms of a maximum *p*-value, p_{max}, which is the number of $Li^+_{(sf)}$ adsorbable on S_8^-. In order to estimate this p_{max}, the closest distance of 200 pm between S_8^- and $Li^+_{(sf)}$ was used, and the p_{max} was estimated to be 43 under several parameters with the so-called utilisation coefficient λ of $\lambda = 1$ conditions. This p_{max} was used to estimate the practical capability of the discharge capacity, taking into account practical values from $\lambda < 1$.

λp could be obtained experimentally as the product of λ and a *p*-value by referring the discharge current data to the discharge capacity equation, and $\lambda p = 16$ was obtained. This $\lambda p = 16$ was greater than 8 times the theoretical discharge capacity of S_8. Since $p_{max} = 43$, in the case of $\lambda = 0.7$, $\lambda p_{max} = 30.1$ was obtained, which was 1.88 times λp of 16 of the experimental discharge capacity. Since $p_{max} = 43$ and practical values of $\lambda > 0.5$, it is expected that the Braga-Goodenough Li-S is to show superior performance compared with that observed in the Braga *et al*. full discharge test.

Conflict of interest: *This paper is free of conflict of interest.*

Appendix

Charge neutrality level in heterojunction

The background and outlines regarding the terminology of 'charge neutrality level' are as follows [8]: The concept of the charge neutrality level appeared more than half a century ago [30,31], but was only observed experimentally in 2000 [32,33]. The charge neutrality level can be regarded as the effective E_f on the semiconductor or insulator side relative to the Schottky barrier, and charge transfer takes place to match the E_f of the metal with the charge neutrality level of the semiconductor or insulator at the interface [22].

The theory of the generalized charge neutrality level, ϕ^G_{CNL}, emerged around 2005 [20-24]. ϕ^G_{CNL} in a heterojunction is characterized by the energy and density of states of the bands of the materials on either side and by orbital hybridisation at their interfaces [20-24]. On the other hand, the conventional ϕ_{CNL} consists of the energy and density of states of the bands for a one-sided material [28]. ϕ_{CNL} cannot take into account the orbital hybridisation at the contact interface and the associated charge transfer. In recent years, problems such as tunnelling leakage currents have arisen due to the increasing integration of electronic devices into nano-devices, and high-*k* insulators have attracted attention as a material to solve these problems. HfO_2, a candidate for the high-*k* insulators, exhibited behaviour that was difficult to resolve with the conventional understanding of heterojunction interfaces, and this ϕ^G_{CNL} succeeded in clarifying this Schottky barrier behaviour [20-24]. ϕ^G_{CNL} can be extended from the metal/insulator Schottky barrier to the evaluation of semiconductor/insulator and semiconductor/ /semiconductor band discontinuities [20-24].

References

[1] K. Waki, *Sulfur/Carbon Composite Electrodes for Lithium-Sulfur Batteries,* Strategy for Technology Development, Proposal paper for Policy Making and Governmental Action toward Low Carbon Societies*,* Center for Low Carbon Society Strategy, Japan Science and Technology Agency, February (2018). https://www.jst.go.jp/lcs/en

[2] M. H. Braga, N. S. Grundish, A. J. Murchison, J. B. Goodenough, Alternative strategy for a safe rechargeable battery, *Energy & Environmental Science* **10** (2017) 331-336. https://dx.doi.org/10.1039/c6ee02888h
[3] D. A. Streingart, V. Viswanathan, Comment on "Alternative strategy for a safe rechargeable battery" by M. H. Braga, N. S. Grundish, A. J. Murchison and J. B. Goodenough, *Energy Environ. Sci*., 2017, 10, 331-336, *Energy & Environmental Science* **11** (2018) 221-222. https://dx.doi.org/10.1039/c7ee01318c
[4] M. H. Braga, A. J. Murchison, J. A. Ferreira, P. Singh, J. B. Goodenough, Glass-amorphous alkali-ion solid electrolytes and their performance in symmetrical cells, *Energy & Environmental Science* **9** (2016) 948-954. https://doi.org/10.1039/C5EE02924D
[5] M. H. Braga, C. M. Subramaniyam, A. J. Murchison, J. B. Goodenough, Nontraditional, Safe, High Voltage Rechargeable Cells of Long Cycle Life, *Journal of the American Chemical Society* **140** (2018) 6343-6352. https://dx.doi.org/10.1021/jacs.8b02322
[6] M. H. Braga, J. E. Oliveira, A. J. Murchison, J. B. Goodenough, Performance of a ferroelectric glass electrolyte in a self-charging electrochemical cell with negative capacitance and resistance, *Applied Physics Reviews* **7** (2020) 011406. https://dx.doi.org/10.1063/1.5132841
[7] M. Sakai, A Reaction Model for Li-Deposition at the Positive Electrode of the Braga-Goodenough Li-S Battery, *Journal of The Electrochemical Society* **167** (2020) 160540. https://dx.doi.org/10.1149/1945-7111/abcf53
[8] M. Sakai, Cathode reaction models for Braga-Goodenough Na-ferrocene and Li-MnO_2 rechargeable batteries, *Journal of Electrochemical Science and Engineering* **13** (2023) 687-711. https://doi.org/10.5599/jese.1704
[9] J. B. Goodenough, M. H. Braga, J. A. Ferreira, J. E. Oliveira and A. J. Murchison, *Self-Charging and/or Self-Cycling Electrochemical Cells,* United States, Patent Application Publication, US 2018/0287222 A1, Oct.4 (2018)
[10] R. W. Gurney, Theory of Electrical Double Layers in Adsorbed Films, *Physical Review Journals Archive* **47** (1935) 479. https://dx.doi.org/10.1103/PhysRev.47.479
[11] R. Gomer, L. W. Swanson, Theory of Field Desorption, *The Journal of Chemical Physics* **38** (1963) 1613-1629. https://doi.org/10.1063/1.1776932
[12] J. Bernard, *Adsorption on Metal Surface, Studies in Surface Science and Catalysis,* Elsevier Sci. Ltd., Amsterdam, 1993, p. 150. ISBN-10: 0444421637
[13] N. Sato, *Electrochemistry at Metal and Semiconductor Electrodes,* Elsevier Sci. B.V., Amsterdam, The Netherlands, 2003, p. 121-126. ISBN 0-444-82806-0
[14] K. J. Vetter, *Electrochemical Kinetics, Theoretical and Experimental Aspects,* Academic Press Inc. New York, 1967, p. 121-128. ISBN 9781483229362
[15] N. Sato, *Electrochemistry at Metal and Semiconductor Electrodes,* Elsevier Sci. B.V., Amsterdam, The Netherlands, 2003, p. 223-225, p. 281-282. ISBN 0-444-82806-0
[16] N. Sato, *Electrode Chemistry,* Nippon Steel Technology Co. Ltd., Tokyo, 1994, **2,** p. 240-258. ISBN 4-930825-06-7 C3043
[17] A. J. Bard and L. R. Faulkner, *Electrochemical Methods, Fundamentals and Applications,* John Wiley & Sons, Inc., 2001, p. 115-117, p. 554-557. ISBN 0-471-04372-9
[18] S. R. Morrison, Two-equivalent and one-equivalent surface states, *Surface Science* **10** (1968) 459-469. https://doi.org/10.1016/0039-6028(68)90112-X
[19] N. Sato, *Electrode Chemistry,* Nippon Steel Technology Co. Ltd., Tokyo, 1994, **2**, p. 108-115. ISBN 4-930825-06-7 C3043
[20] T. Nakayama, K. Shiraishi, S. Miyazaki, Y. Akasaka, K. Torii, P. Ahmet, K. Ohmori, N. Umezawa, H. Watanabe, T. Chikyow, Y. Nara, A. Ohta, H. Iwai, K. Yamada, T. Nakaoka, Physics of Metal/High-k Interfaces, *ECS Transactions* **3(3)** (2006) 129. https://doi.org/10.1149/1.2355705

[21] K.Shiraishi, Y. Akasaka, S. Miyazaki, T. Nakayama, T. Nakaoka, G. Nakamura, K. Torii, H. Furutou, A.Ohta, P. Ahmet, K.Ohmori, H.Watanabe, T. Chikyow, M. L. Green, Y. Nara and K. Yamada, *Technical Digest of IEEE International Electron Devices Meeting*, Washington D.C., USA, 2005, p. 43-46. ISBN 9780780392687
[22] T. Nakayama, K. Shiraishi, Physics of Metal/Insulator Interfaces: Schottky Barrier and Atom Intermixing, *Hyomen Kagaku* **28(1)** (2007) 28-33.https://dx.doi.org/10.1380/jsssj.28.28 (In Japanese)
[23] K. Shiraishi, T. Nakayama, Universal Theory of Metal/Dielectric Interfaces, *Hyomen Kagaku* **29(2)** (2008) 92-98.. https://dx.doi.org/10.1380/jsssj.29.92 (In Japanese)
[24] T. Nakayama, Y. Kangawa, K. Shiraishi, *Atomic Structures and Electronic Properties of Semiconductor Interfaces in Comprehensive Semiconductor Science and Technology,* P. Bhattacharya, R. Fornari, H. Kamimura, Eds, Elsevier Sci. B.V., Amsterdam, The Netherlands, 2011, p. 157-161. ISBN 978-0-444-53153-7
[25] N. Sato, *Electrochemistry at Metal and Semiconductor Electrodes,* Elsevier Sci. B.V., Amsterdam, The Netherlands, 2003, p. 35-37. ISBN 0-444-82806-0
[26] N. Sato, *Electrochemistry at Metal and Semiconductor Electrodes,* Elsevier Sci. B.V., Amsterdam, The Netherlands, 2003, p. 39-41, p. 44-45. ISBN 0-444-82806-0
[27] T. Nakayama, Band offsets: the charge transfer effect, *Physica B: Condensed Matter* **191** (1993) 16-22. https://dx.doi.org/ 10.1016/0921-4526(93)90175-6
[28] M. Cardona, N. E. Christensen, Acoustic deformation potentials and heterostructure band offsets in semiconductors, *Physical Review* B **35** (1987) 6182. https://dx.doi.org/10.1103/PhysRevB.35.6182
[29] S. J. Rettig, J. Trotter, Refinement of the structure of orthorhombic sulfur, α-S_8, *Acta Crystallographica Section C: Structural Chemistry* **43** (1987) 2260-2262. https://doi.org/10.1107/S0108270187088152
[30] W. J. Bardeen, Surface States and Rectification at a Metal Semi-Conductor Contact*, Physical Review Journals Archive* **71(10)** (1947) 717. https://dx.doi.org/10.1103/PhysRev.71.717
[31] A. M. Cowley, S. M. Sze, Surface States and Barrier Height of Metal-Semiconductor Systems, *Journal of Applied Physics* **36(10)** (1965) 3212-3220. https://doi.org/10.1063/1.1702952
[32] S. Hara, The Schottky limit and a charge neutrality level found on metal/6H-SiC interfaces, *Hyomen Kagaku* **21(12)** (2000) 791-799. (In Japanese). https://dx.doi.org/10.1380/jsssj.21.791
[33] S. Hara, The Schottky limit and a charge neutrality level found on metal/6H-SiC interfaces, *Surface Science* **494(3)** (2001) L805-L810. https://doi.org/10.1016/S0039-6028(01)01596-5